Agricultural and Forest Meteorology 331 (2023) 109348

Contents lists available at ScienceDirect

Agricultural and Forest Meteorology

journal homepage: www.elsevier.com/locate/agrformet

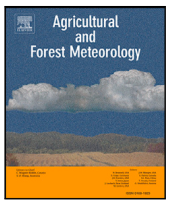

Tree volume estimation with terrestrial laser scanning — Testing for bias in a 3D virtual environment

Meinrad Abegg [a,c,*], Ruedi Bösch [b], Daniel Kükenbrink [b], Felix Morsdorf [c]

[a] Forest Resources and Management, Swiss Federal Institute for Forest, Snow and Landscape Research WSL, Zürcherstrasse 111, CH-8903 Birmensdorf, Switzerland
[b] Land Change Science, Swiss Federal Institute for Forest, Snow and Landscape Research WSL, Zürcherstrasse 111, CH-8903 Birmensdorf, Switzerland
[c] Remote Sensing Laboratories, Department of Geography, University of Zurich, Winterthurerstrasse 190, CH-8057 Zürich, Switzerland

ARTICLE INFO

Keywords:
Forest inventory
Simulation
Terrestrial laser scanning
Tree volume estimation

ABSTRACT

Tree volume is a key feature in forest monitoring, delivering information, such as wood availability or forest carbon balance. To date, tree volume, i.e. the total volume of the above ground woody parts of a tree, cannot be measured directly with conventional tools. Terrestrial laser scanning (TLS) offers the potential to directly measure tree volume. However, its application in forest monitoring requires a profound understanding of the precision and accuracy of retrieval approaches. In this study, we present a simulation environment for evaluating TLS application in forest inventories. We investigate the influence of understorey density, scanner placement and TLS sensor type on volume estimation of tree parts of varying diameters. Using information from 30 sample plots from the Swiss NFI to simulate 197 sample trees, we evaluate three understorey densities, five scanner locations and their combinations and three realistic and one hypothetic (geometric scanning) TLS sensor types. We show that tree volume estimates from point clouds are biased to certain extent: from about 25% for small trees to a few percent for larger trees above 40 cm diameter at breast height (DBH). Especially small tree parts (diameters < 7 cm) lack accurate and precise estimation. In small trees with 12 cm DBH they are overestimated by 110% in average with a high variation, whereas they are underestimated in large trees, i.e. with DBH ≥ 75 cm, by 50% in average. Volume estimation of small tree parts is subject to physical limits of TLS, however the estimation of volume of large tree parts could be feasible with appropriate TLS settings and field protocols. Nevertheless, tree volume estimation using TLS must be understood in greater depth before it can be applied regularly in forest inventories.

1. Introduction

National forest inventories (NFI) are an established process to provide data, on the national and the international level, on forests and their contribution to human welfare (FOREST EUROPE, 2015; MacDicken et al., 2016). The impact of global climate change leads to greater interest in the role of forests as carbon sinks or sources (Pan et al., 2011). Tree volume, i.e. the total volume of the above ground woody parts of a tree, which is closely connected to tree biomass and carbon stock, is one of the most important forest features forming the basis of NFI reporting. With traditional NFI tools, such as the calliper to measure tree diameters, tree volume cannot be measured directly. Volume and biomass are derived with allometric models using tree diameter at breast height (DBH) as the most important explanatory variable (Chave et al., 2014; Brassel and Lischke, 2001). However, these models suffer from the lack of variables describing the tree above the breast height. Sometimes tree height and the upper diameter of the tree stem can be measured in the field, providing more accurate volume estimates for the tree stem. Nonetheless, for the volume of tree branches, allometric relationships between the stem and the tree crown (branches) are applied. In Switzerland these models are based on historical destructive sampling data (Brassel and Lischke, 2001), that is not completely representative for the whole country. Yet, from an inventory statistical point of view, calibration of volume models on trees from the sampling grid of the NFI would be beneficial. Saarinen et al. (2017) or Calders et al. (2020) point out that there is a growing interest in utilizing terrestrial laser scanning (TLS) as a basis for developing stem volume models. TLS is a technology that could provide accurate measurements of complete trees in a high degree of detail. For inventory purposes, however, it is crucial to know the accuracy and precision of TLS-based volume estimates aiming for bias-free estimates of tree volume. Furthermore, additional measurements usually lead to additional costs. Hence, a possible improvement of volume estimations

* Corresponding author at: Forest Resources and Management, Swiss Federal Institute for Forest, Snow and Landscape Research WSL, Zürcherstrasse 111, CH-8903 Birmensdorf, Switzerland.
E-mail address: meinrad.abegg@wsl.ch (M. Abegg).

https://doi.org/10.1016/j.agrformet.2023.109348
Received 1 July 2022; Received in revised form 23 January 2023; Accepted 27 January 2023
Available online 31 January 2023

with TLS measurements compared with the current allometric approach must be proven before TLS can be implemented in the NFI workflow.

Demol et al. (2021) compared TLS-derived tree volume to 65 trees destructively measured trees in Belgium. Kükenbrink et al. (2021) compared TLS-derived biomass estimation of 55 urban trees with allometric equations and total tree weight. Saarinen et al. (2017) investigated the applicability of TLS in the development of new stem volume models (equations) based on diameter measurements through cylinder-fitting along the stem on 9 destructively sampled trees. Calders et al. (2015) compared biomass estimates applying the software treeQSM (Raumonen et al., 2013) on TLS point clouds of 74 destructively sampled trees in an Australian Eucalyptus forest. Bremer et al. (2013) investigated the influence of various TLS scanning settings (angular resolution, single and multiple scanning) by manipulating the point cloud of one scanned tree from 3 different scanning locations. These studies give insight in TLS application characteristics in specific situations. However, every intended TLS application might have its own peculiarities, owing to the forest structure, the TLS device or the applied algorithms.

As point cloud acquisitions and collecting meaningful ground truth data, e.g. by destructive sampling, are labour intensive, generating TLS readings from synthetic forest plots is a way of evaluating TLS approaches at a relatively low cost. LiDAR in forested environments has been simulated before (e.g. Lewis, 1999; Lovell et al., 2005; Kukko and Hyyppä, 2007; Van der Zande et al., 2008; Morsdorf et al., 2009; Disney et al., 2010; Gastellu-Etchegorry et al., 2015; Liu et al., 2022), however, most of these approaches are focussed on airborne LiDAR simulations with different observation geometries and distances. Nevertheless some authors (e.g. Binney and Sukhatme, 2009; Disney et al., 2012; Raumonen et al., 2013; Wang et al., 2022), simulate TLS data of one tree (or tree part) to validate approaches of tree reconstruction or plant movement quantification from forest TLS point clouds.

As stated by various authors (e.g. Watt and Donoghue, 2005; Van der Zande et al., 2006; Trochta et al., 2013), occlusion is a major problem for TLS in forests. One way to overcome this problem is by combining multiple point clouds from different locations in a stand. Different scanner placement patterns are described in the literature (e.g. Watt and Donoghue, 2005; Wezyk et al., 2007; Yang et al., 2013; Liang et al., 2016). Trochta et al. (2013) evaluated different distances between scanners and trees for an optimal stem recognition, whereas Van der Zande et al. (2008) compared 3 scanner position combinations in 3 stands. Saarinen et al. (2017) tested different distances between scanner and tree and evaluated the influence of multiple scanning on the improvement of the stem volume estimation. A more extensive evaluation of possible scanning positions in a wide range of stand properties was conducted by Abegg et al. (2017). However, they assessed forest stands and scanner placement in terms of optimal visibility only, in a highly abstract virtual environment.

For the application of TLS in forest inventories, the parameters influencing LiDAR point cloud characteristics, such as stand condition, stem and understorey density, TLS device, scanner placement and tree shape, must be understood in detail for estimates including tree volume. The added cost and complexity of introducing TLS to NFIs have to be offset by an increase in wood volume retrieval quality. The latter has the dimensions precision (variation), accuracy (bias) and extent (e.g. by sampling more trees and/or more parts of trees).

In this study, we introduce an evaluation approach for TLS applications in forest inventories and we use tree volume as the target variable. To confirm the hypothesis of Abegg et al. (2021) and Demol et al. (2022), that only larger object diameters can be represented by TLS, the volume of the trees was divided into merchantable wood, which comprises all above-ground parts with a diameter ≥ 7 cm, and the wood of small branches and the tree top, which comprises the above-ground tree parts < 7 cm in diameter.

Hence, the goal of this study is to: (i) implement a TLS simulation environment for forest inventories, (ii) compare different TLS sensor types, (iii) determine the influence of object diameters on volume estimates, (iv) check whether understorey density affects the quality of tree volume estimates and (v) test whether including multiple scanner locations improves the precision of volume estimates.

2. Materials and methods

2.1. Simulated forest stands

2.1.1. NFI forest and tree information

The Swiss NFI collects data on a regular sampling grid with a mesh size of 1.41 km over the entire area of Switzerland. This provides data on forest stands, trees and site conditions for 6357 forest sample plots with a wide range of features. Data on trees starting at 10 cm height are measured on circular sample plots. However, the location of the trees is only recorded for the ones with a diameter at breast height (DBH) of at least 12 cm.

For our study, we used information on the trees with DBH ≥ 12 cm, which are the basis for the forest resources estimations. The sample plot covers a horizontal circle with an area of 200 m^2. Furthermore, we focussed on deciduous trees where the crown shape represents a complex geometry and more biomass is stored in the branches compared to coniferous trees (Brassel and Lischke, 2001). In order to evaluate the influence of understorey on laser scanning, we selected only single-layered stands, where a virtual understorey could be added without overlap with the tree crowns. The selected sample plots for simulations consisted of only standing and living trees.

The forest ground was defined as a horizontal and plane surface.

As tree information, we used the location of the trees on the NFI sample plots and the DBH directly, and the tree height and crown length in a derived form. The tree height was derived from the estimated stand height. According to the field manual of the Swiss NFI (Keller, 2011), tree crown length is assigned to one of three classes: more than half the tree height, between half the tree height and one quarter of the tree height, and less than one quarter of the tree height. Tree crown length was set to the given crown length from the field assessment with a uniformly distributed variation within the crown length classes. However, we limited crown length to start above the understorey and cover at least 20% of the tree height.

2.1.2. 3D tree model

The object of this study is to evaluate the tree volume estimation by TLS under the influence of TLS sensor type, understorey and scanning protocol. The sapling tree add-on for the software Blender, based on the work of Weber and Penn (1995), makes it possible to generate trees of a wide range of shapes and tree crown structures. The sapling tree add-on produces tree shapes with conical stems and branches up to six branching levels. The stem/branch length, curvature and direction can be specified for each branching level up to level four. The branches are distributed on a parent branch/stem in a helical way. We parametrized the tree model for the sample trees with volume estimation as displayed in Table A.1 in the Appendix, in order to produce trees like the ones shown in Fig. 1. The volumes of these 3D tree models are in accordance with the volumes of deciduous trees with the same DBH derived from allometries of the Swiss NFI. For the understorey tree model, a similar parametrization was chosen (see Table A.2 in the Appendix) with varying number of branching levels (1, 2 and 3).

2.2. TLS simulation and point cloud processing

2.2.1. Simulation of laser scanning with blender

Blender (Blender Online Community, 2015), a 3D content creation suite, is designed to render images and movies of complex virtual 3D scenes. It offers a large toolbox to create 3D objects and define their light interaction properties. The add-on BlenSor (Gschwandtner et al., 2011) enables access to internal parts of Blender where the interaction of light rays with 3D objects is calculated. Originally, the BlenSor add-on was designed for simulations of various vehicle-mounted sensors. Abegg et al. (2021) developed it further to simulate realistic properties of three state-of-the-art terrestrial laser scanners.

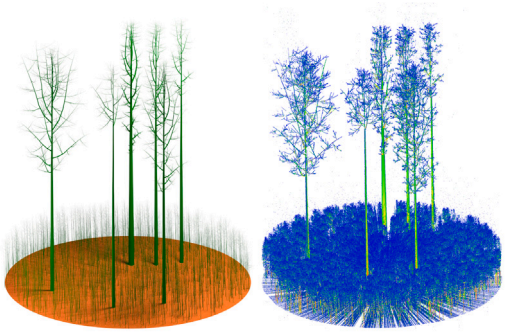

Fig. 1. Simulated sample plot with trees and understorey (32 000 saplings per hectare). Left side: rendered image of the stand 3D model. Right side: Point cloud of a simulated terrestrial laserscan (R-system) from the plot centre. The point cloud colours refer to the reflected light intensity: blue equals low intensity, green equals medium intensity and red equals high intensity.

Implemented features were the prefiltering of points, the distance deviation of points from the objects surfaces and the triggering of multiple echoes from one laser pulse in cases where the Gaussian shaped virtual laser pulse intersects with multiple objects. Prefiltering, as used here, means removing certain ambiguous points from the point cloud by the scanning device already during scanning. Furthermore, any angular resolution, laser beam diameter upon exit from the device, and beam divergence can all be simulated. In this publication, we additionally implemented Lambertian scattering, i.e. reflected light intensity, with values from 0 to 1, follows the cosine of the incident angle on the objects' surface. This on the one hand uses more realistic reflected laser pulse energy for the triggering and on the other hand delivers light intensity for each point in the resulting point cloud (see Fig. 1).

2.2.2. Point cloud processing

The simulation of laser scanning with an angular resolution of 0.04° is computationally demanding. In order to reduce the calculation time, the scan of one scene was divided into 150 longitudinal (horizontal) slices. The simulation of one slice loaded the complete 3D forest scene, to only scan 2.4° in latitudinal direction, covering the whole section from the zenith to the lowest scanning angle towards the ground. This enables the TLS simulation of each slice of the scene separately, via parallel processing on a high performance computer. The point cloud for one scanning position was then recomposed from the different slices. Since one slice was simulated with the complete 3D forest scene and the scanning angles were defined continuously for all slices, the composed point cloud was exactly the same as if simulated for the whole 360° in one take. Since the exact location of the simulated scans was known, single scan point clouds could be easily composed to multiple scanning locations. With the known positions of the trees, height of the understorey layer and extent of the tree crowns, the trees were clipped automatically from the point cloud, without the need for an error-prone manual or automated segmentation.

2.3. Volume calculation

In this study, we compared the volume of the 3D tree models (see Section 2.1.2) with the tree volumes calculated from the simulated point clouds.

The volume derivation of the 3D model works as follows: The Blender sapling tree add-on defines trees as a Bezier curve with diameters assigned along the curve. In Blender, the diameter, which describes a tube-like shape, is named bevel. For the processing of the tree model, each branch is labelled with a separate identifier. With a Blender native function, we converted the curves and their corresponding bevels to closed, triangulated meshes for each tree part (stem, branches, twigs). The defined trees still had overlapping parts at each branch start. The reason is, that the branch was originally defined as a line (curve) with no diameter, so the origin of a branch was always in the centre of the parent branch/stem. We removed these overlapping parts using a Blender native functionality to avoid double accounting for their volume.

To investigate the influence of the object diameter on the volume estimate, the branches were cut off at 7 cm (threshold for merchantable wood). This enabled us to calculate the total tree volume, the volume of tree parts with diameters above the threshold (merchantable wood) and their difference (the volume of small tree parts). We used geometric functions to iterate through the stem and branches to search the diameter threshold.

The volume of the trees was calculated according to the procedure described by Zhang and Chen (2001): each triangle of the object's mesh structure represents a tetrahedron with the origin of the scene and hence a specific volume. The volume of these tetrahedrons can be positive or negative relative to the direction of the normal vector. The sum of all (positive and negative) volumes equals the volume of the whole tree.

The tree volume derived from the point cloud was calculated according to Raumonen et al. (2011, 2013) with an open-source Matlab script called treeQSM. TreeQSM was tested with field measurements and with simulated data (Brede et al., 2019; Lau et al., 2019; Pitkänen et al., 2019; Calders et al., 2015; Disney et al., 2012). TreeQSM can run its volume estimations with different starting parameters, influencing the outcome of the estimate. We tested two parameters each for minimum patch size of the cover sets in the second cover (0.03, 0.04) and relative length (length/radius) of the cylinders to be fitted (2, 4). The rest of the starting parameters were set to a fixed value: 0.1 as patch size of the first uniform-size cover, 0.1 as the maximum cover set size in the stem's base in the second cover and 3 as the relative radius for outlier point filtering.

2.4. Workflow of simulation and analysis

2.4.1. Preparatory steps: selection of the parameters to be tested

We selected 30 sample plots which fulfil the following conditions: only deciduous, living and standing trees of various diameters (12–87 cm) in single-layered stands with various tree numbers per plot (2–17). The diameter distribution of the sample trees is displayed in Fig. 2.

The five scanner locations were selected manually so that locations were equally distributed within the sample plot and covered various aspects of the trees, following the recommendations of Abegg et al. (2017). One scanner location was set to the centre of the sample plot. The five scanner locations on a 200 m^2 sample plot lead to a scanner location density of 50 scanner locations per hectare.

We selected three different densities of the understorey layer: 0 (no understorey at all), 11 200 and 32 000 individuals per hectare. These densities were implemented on each of the 30 sample plots.

The angular resolution of the scanner was set to 0.04° and the height of the scanner above ground to 0.98 m. For the comparison of different scanning systems, we implemented four different signal triggering approaches according to Abegg et al. (2021). The 'geometric' scanning system is a hypothetical laser scanner, scanning with an infinitesimally small laser beam diameter producing no noise. The 'L-system' is based on a Leica BLK360 scanner. It is a discrete TLS system which triggers one point per laser pulse, even though being a time of flight LiDAR system. It performs prefiltering of laser pulses hitting multiple objects. The 'F-system', based on a Faro^{3D} is a discrete TLS system as well. When its laser pulses intersect with multiple objects, it either prefilters the signal, returning no point, or it displays two kinds of distance deviation from the actual objects, depending on the distance of the objects to each other. This behaviour partly results from being a phase shift LiDAR system. The signal triggering of the 'R-system' is

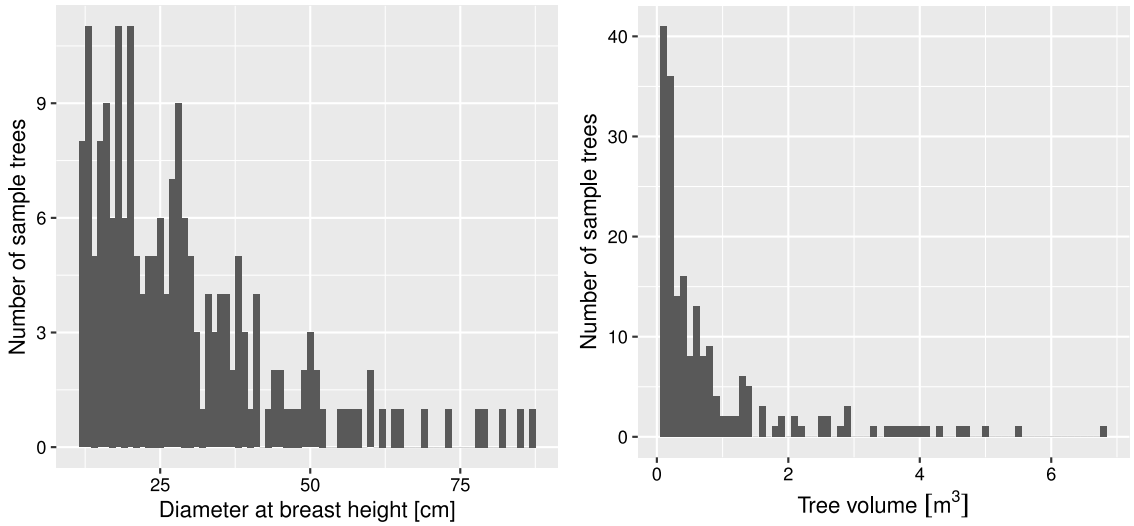

Fig. 2. Diameter and total tree volume distribution of the scanned sample trees. The bin size of the tree diameters is 1 cm and 0.1 m^3 for the tree volumes.

Table 1
Beam diameters, divergences and distance measurement uncertainty of the simulated TLS scanning systems, according to the specifications of their respective real-life models following the $1/e^2$ definition.

Simulated TLS system	Beam diameter at exit [mm]	Beam divergence [mrad]	Uncertainty in distance measurement [mm]
Geometric	0	0	0
L-system	3.82	0.68	4
F-system	4.24	0.54	3
R-system	6.5	0.3	3

based on a Riegl VZ-1000 system. It has noise properties similar to the F-system. Since it is able to produce multiple echoes from one laser pulse, as a time of flight LiDAR system, some points laterally deviate from the objects surfaces, because their laser beam cones only touched the object at their fringes (for details see Abegg et al., 2021).

Even though the simulated scanning systems are an abstraction of real-life models, we chose their laser beam properties and distance noise (see Table 1) according to available information on these scanning systems. The parameters for the R-system refer to a Riegl VZ-400 system which is more common to forest applications than the VZ-1000. The uncertainty in distance measurement follows the data sheets of the manufacturers, nevertheless their specification of 'range accuracy' (actually meaning precision) or 'noise' might not be exactly the same as in the simulation. We did not simulate a general bias, i.e. lack of accuracy, in the distance measurement even though we observed such behaviour, dependent on the surface properties, in lab tests.

2.4.2. Preparation and scanning of 3D sample plot

The 3D scene to be scanned was composed of the previously defined and measured 3D tree models (see Sections 2.1.1 and 2.1.2) which were linked to the scene and a forest ground containing the understorey as a particle system. The particle system is a Blender functionality, similar to linking existing tree models to a scene, defining the random location of instances of any previously defined object. This reduces memory demand considerably, allowing scenes to consist of more than 10,000 objects. We used the particle system to fill the Blender forest scene with instances of three sapling tree models (see Section 2.1.2) according to the understorey density per hectare to be evaluated. The sapling trees consisted of individuals with one of three branching levels (1, 2 and 3), which were then randomly selected to compose the understorey. The understorey height was set to 4 m. Additionally, the understorey trees were not placed within a buffer of 0.5 m around the locations of the sample trees and the scanner. Our goal was to compare TLS scans of the same scenes with and without an understorey layer (see Section 2.4.1). In brief, for each scanner location and tested understorey density, the virtual sample plot scenes were scanned with the before-defined TLS specifications.

2.4.3. Preparation and analysis of point cloud

The single scan point clouds were then registered to a multiple-scan point cloud combining the point clouds of the five scanner locations on each sample plot in the following way: combination of the two opposite scanner locations, combination of the two opposite scanner locations with the central location, combination of all scanner locations without the central location, and combination of all scanner locations. Since the scanner location in the simulation was known precisely, registration did not lead to additional noise in the point clouds.

The trees were clipped from the point clouds using the known location, height, crown base height and understorey height. With the before described combinations of scanning systems, understorey densities, scanner location and scanner location combinations, this resulted in a total of 26 004 tree point clouds.

Often point clouds are filtered in one or the other way before further processing. Especially for scanning systems similar to the here presented R-system, filtering is applied, since without filtering the point clouds tend to be very noisy due to the high sensitivity of these systems. We applied a filtering of the R-system point clouds, that removes all points with an intensity below 0.1. Intensity as used here, is the potentially reflected energy, with values between 0 and 1, of a laser pulse hitting an objects surface, dependent on the incident angle and the fraction of the laser beam that hits the object.

The tree point clouds were then analysed in Matlab using treeQSM (Raumonen et al., 2013), providing the tree volume above and below the diameter threshold of 7 cm.

3. Results

3.1. Influence of scanning system on volume estimations

As described in Abegg et al. (2021), the TLS simulation environment can simulate different LiDAR echo triggering systems. For this study, we tested three TLS scanner types (L-system, F-system, R-system) based on real TLS devices and a geometric scanning (using an infinitesimally small laser beam) to compare the results of the realistic systems with a "perfect" scanning system. The L-system, based on a Leica BLK360, prefilters ambiguous LiDAR pulses reflected by multiple objects (mixed pixel effect). Similarly, the F-system, based on a Faro^{3D}, includes

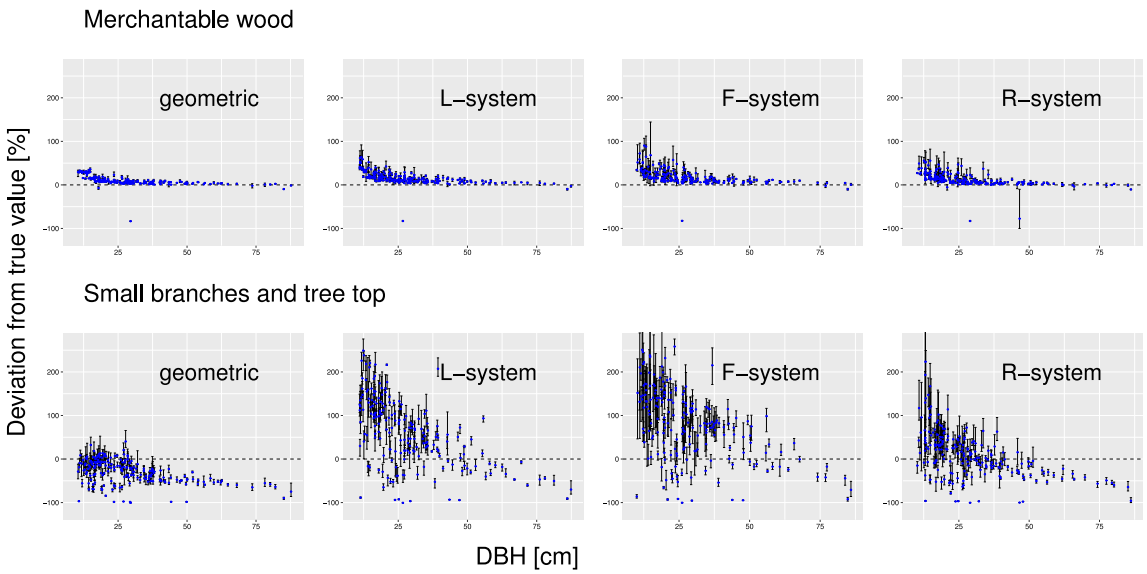

Fig. 3. Influence of the scanning system on the quality of volume estimations from point clouds of five scanning positions in simulated forest stands with no understorey. For each tree point cloud, the deviation (bias) of the QSM outputs compared with the actual volume of the 3D tree model is displayed (black whiskers for the ranges, blue dots for the mean deviations). The upper panels show the bias of the volume estimates for merchantable wood (diameter ≥ 7 cm), and the lower panels show the bias of the volume for small branches and the tree top (diameter < 7 cm). The left panels show the outcome of geometric scanning (with infinitesimally small laser beams), whereas the right panels show the outcome of realistic signal triggering approaches.

prefiltering of ambiguous reflections, but also performs distance deviation from certain mixed pixel effects that are not prefiltered. The R-system, based on a Riegl scanner, has no prefiltering, it can trigger multiple echoes in mixed pixel situations, using more information of the scanned forest scene and allowing it to apply custom filtering as a post processing step. The point cloud of the R-system was filtered as described in Section 2.4.1.

Fig. 3 shows that the QSM starting parameters similarly influence the variation in the QSM estimation for all realistic systems, i.e. the deviation of the volume estimates of small trees from the (true) 3D model volume varies more than with larger trees. For merchantable wood (diameter ≥ 7 cm), all scanning systems perform similarly, with a slightly higher variation in the realistic systems, especially the F-system (more complex noise generation, but no intensity filtering). All systems, including geometric scanning, result in a slight overestimation of the wood volume, especially for small trees. Concerning the volume estimate of small branches and the tree top (tree parts with diameters < 7 cm), the QSMs running on point clouds, generated by the realistic systems, strongly overestimate the true volume, especially for smaller trees (e.g. DBH less than 50 cm). The QSMs running on point clouds from geometric scans mostly underestimate the wood volume. Another difference between estimates based on geometric scanning and realistic systems is the larger variation, within one tree and between trees of the same size. Additionally there is also a difference between the realistic systems. The R-system (noise simulation, multiple echo triggering and posterior intensity filtering) performs best within the realistic systems. Second is the L-system (single echo triggering, prefiltering) followed by the F-system (single echo triggering, weak prefiltering, noise simulation). In brief, the realistic scanning systems perform similarly with a slight advantage of the R- and L-systems. Large discrepancies to geometric scanning occur mostly for small branches and tree top.

Fig. 4 shows the number of points per tree surface area for the different scanning systems (single scan). There seems to be no visible difference between the realistic scanner systems. Even the R-system, able to trigger multiple points per laser pulse, is similar to the others. Since all three realistic systems perform similarly, we display in the further analysis the scanning system with the least complex noise structure, the L-system (single echo triggering and prefiltering of some mixed pixel effects).

3.2. Influence of object size on volume estimation

Fig. 5 shows the bias of wood volume estimates, derived by QSM, applied to the simulated point clouds of trees scanned from multiple scanning positions with the L-system. For merchantable wood (diameter ≥ 7 cm) the QSM consistently overestimates the true volume. The bias of the volume estimate in relation to the respective tree volume is considerably high (up to a mean of 25%), especially for small trees. However, absolute values in m^3 are larger for big trees. When small branches and the tree top (diameter < 7 cm) are considered, the QSM derived values show considerable over- or under-estimations, depending on the tree size. Furthermore, the variation in the relative bias of small branches and the tree top is far higher compared with the values for merchantable wood.

3.3. Influence of understorey on volume estimations

Fig. 6 shows the potential influence of understorey density on the volume estimates for point clouds from five different locations scanned with the L-system. In the simulations, there seems to be no influence of the understorey, even with understorey stem densities of 32 000 pieces per hectare. Also the ratio of failed volume calculations, due to severe occlusion of the tree stems, remains the same. This might be due to the fact, that even 32 000 saplings per hectare, result in around 3 pieces per m^2. And if they do not carry leaves, occlusion is rather weak (as a visual inspection of the point clouds confirms).

3.4. Influence of multiple scanner positions on volume estimations

Fig. 7 compares the volume estimates of point clouds with different numbers of combined scanner locations simulated with the L-system. Among the point clouds from multiple scanning locations there are only small visible differences. For merchantable wood, the estimates become more stable with more combined scanner positions. Interestingly, the estimates for small branches and tree top, become less stable with more combined scanner positions. Furthermore they slightly tend to an overestimation compared to the single scans. Additionally, the number of failed QSMs, due to severe occlusion of the tree stem, for single scan positions is higher than the number of failed QSMs for the combined scanner locations (4.5% vs 0.2%).

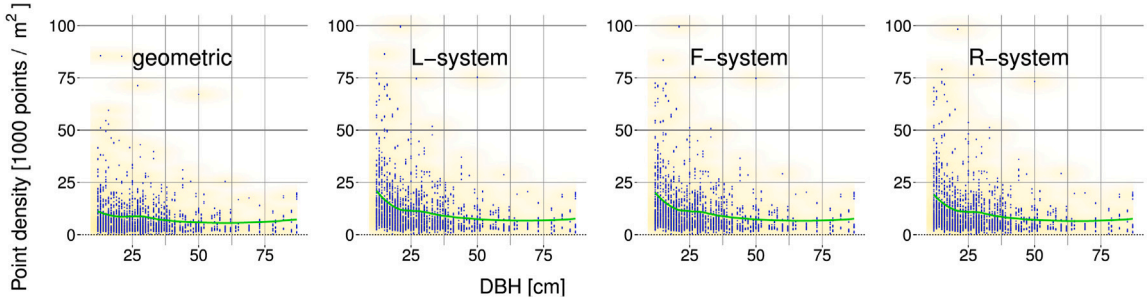

Fig. 4. Influence of the scanning system and the tree diameter on breast height (DBH) on the number of points on the tree surface of point clouds from one scanning positions in simulated forest stands. The green line is a "loess" smoothing line on the data (R Core Team, 2017). The left panel shows the outcome of geometric scanning (with infinitesimally small laser beams), whereas the right panels show the outcome of realistic signal triggering approaches.

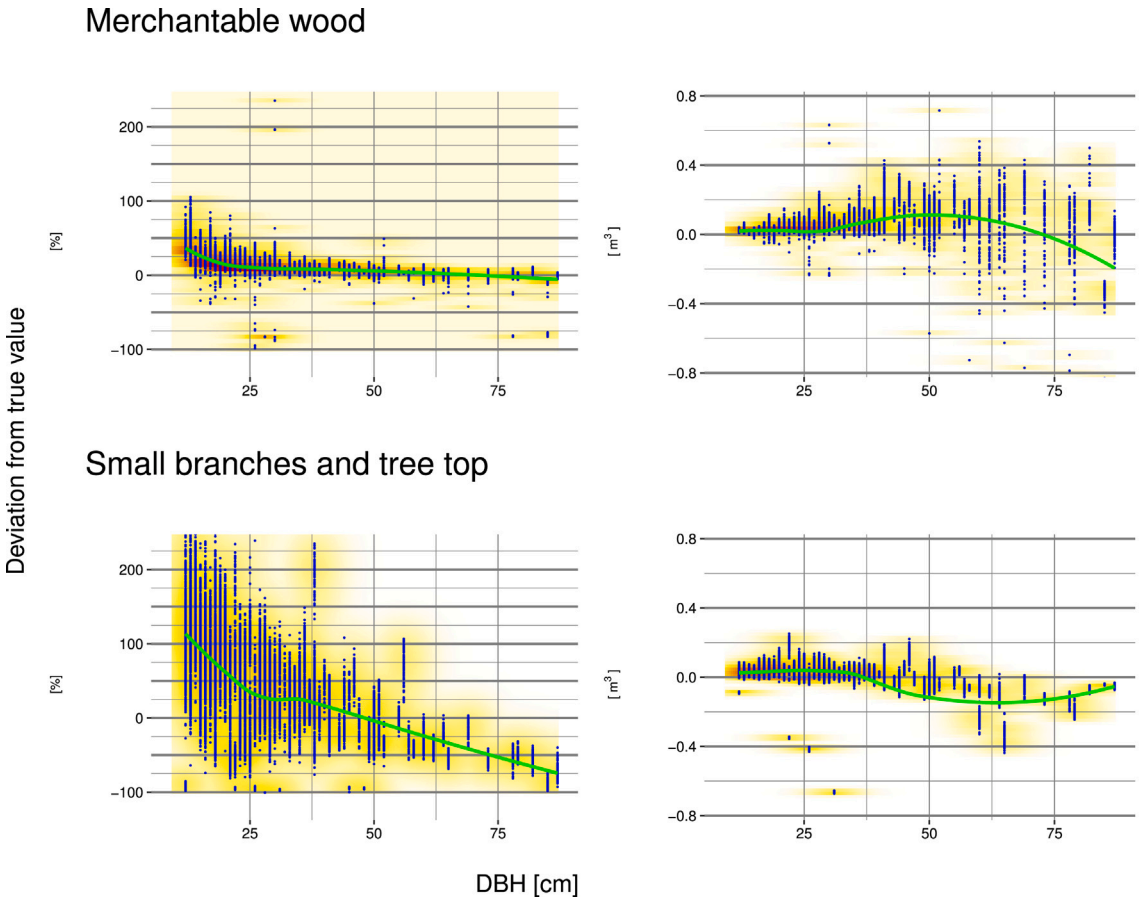

Fig. 5. Influence of object size on the quality of volume estimates from point clouds with multiple scanning positions in simulated stands by the L-system. For each tree point cloud, the range of deviation (bias) of the QSM output compared with the actual volume of the 3D model is displayed as blue dots in percentage [%] and absolute values [m^3]. The green line is a "loess" smoothing line on the data (R Core Team, 2017). The upper panels show the bias of the volume estimates for merchantable wood (diameter ≥ 7 cm), and the lower panels show the bias of volume estimates for small branches and the tree top (diameter < 7 cm).

4. Discussion

In this study, we present a simulation approach which enables the evaluation of TLS application in forest inventories. As an example, we investigate the influence of TLS device, understorey density and scanner placement on the quality of tree volume estimates in deciduous forest stands without foliage.

A wide variety of possible TLS applications in forest inventories can be tested with the presented simulation environment. In particular, specific situations can be investigated under different conditions, e.g. with and without understorey or with different TLS devices. Another advantage of the simulation is the availability of a perfect "ground truth", i.e. the exact volume of the used tree models is known.

Nevertheless, simulating realistic forest environments can be very complex and the implementation effort is considerable. Further, simulations are always an abstraction of reality, and the results of such simulations should therefore be interpreted carefully. For this study, we chose an easily parametrizable tree model to be used within the 3D content creation suite Blender. It enables influencing a wide range of tree properties, such as diameter, tapering, length, curvature and orientation of the stem and branches. However, the difference to real tree structures is its helical branch placement on parent branches/stems. This structure is encountered in real trees as well (alternate branching), but does not cover all existing branching structures (e.g., opposite branching, whorled branching). Nevertheless, also with the helical branching structure any branch density can be emulated. Furthermore,

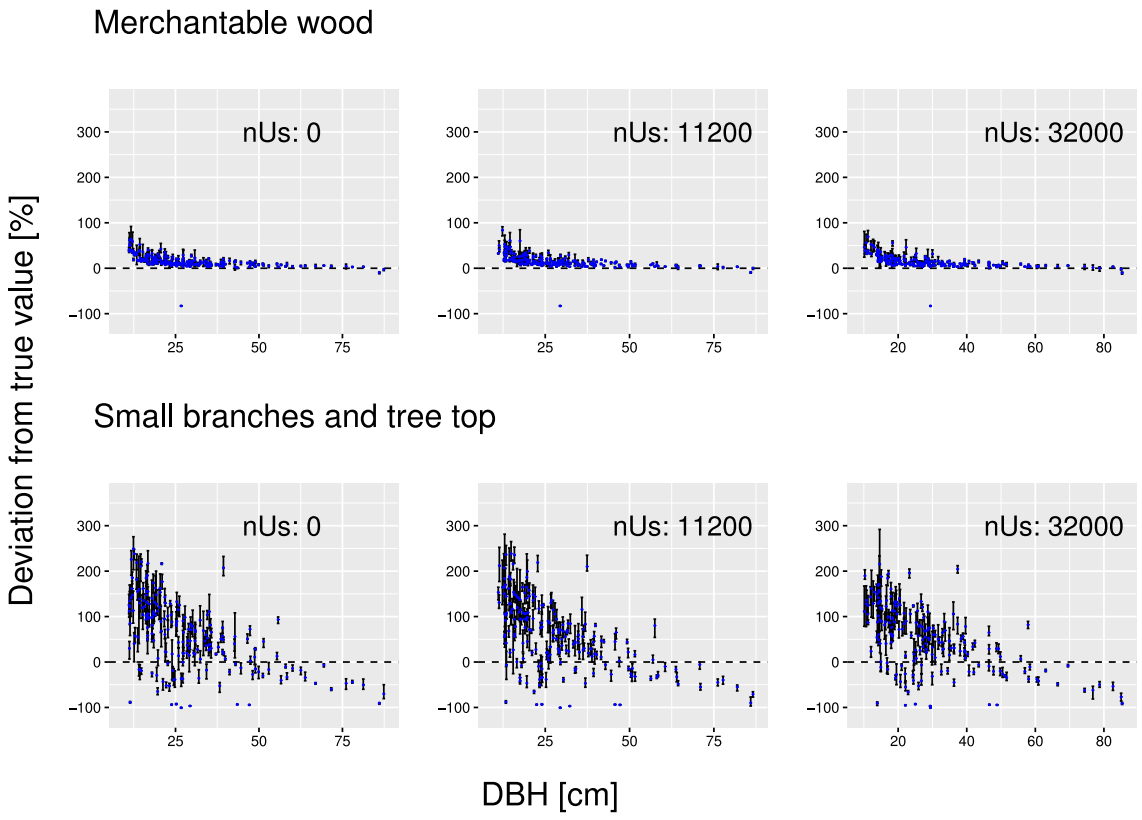

Fig. 6. Influence of understorey density on the quality of volume estimates from point clouds generated with the L-system. For each tree point cloud, the range of deviation (bias) of the QSM output compared with the actual volume of the 3D model is displayed. The upper panels show the bias of the volume estimates for merchantable wood (diameter ≥ 7 cm), and the lower panels show the bias of the volume estimates for small branches and the tree top (diameter < 7 cm). From left to right, an increasing stem number (nUs) of understorey trees (4 m in height) is shown: 0, 11 200 and 32 000 pieces per hectare. The blue dots represent the mean deviations of QSM volume estimates based on tree point clouds, and the whiskers represent the range of volume estimates resulting from the use of different QSM starting parameters.

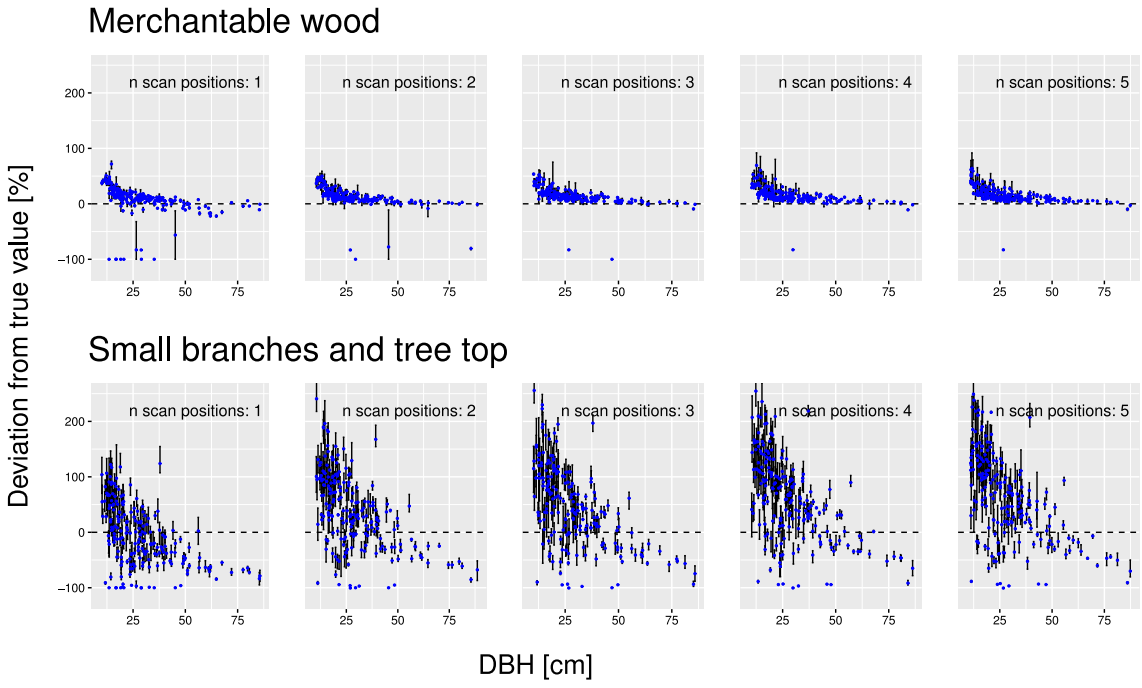

Fig. 7. Relative bias of QSM volume estimates in simulated with the L-system in forest environments with different numbers of combined scanning locations, for merchantable wood (≥ 7 cm diameter) and small branches/tree top (< 7 cm diameter). The blue dots represent the mean deviations of QSM volume estimates based on tree point clouds and the whiskers represent the range of volume estimate resulting from the use of different QSM starting parameters.

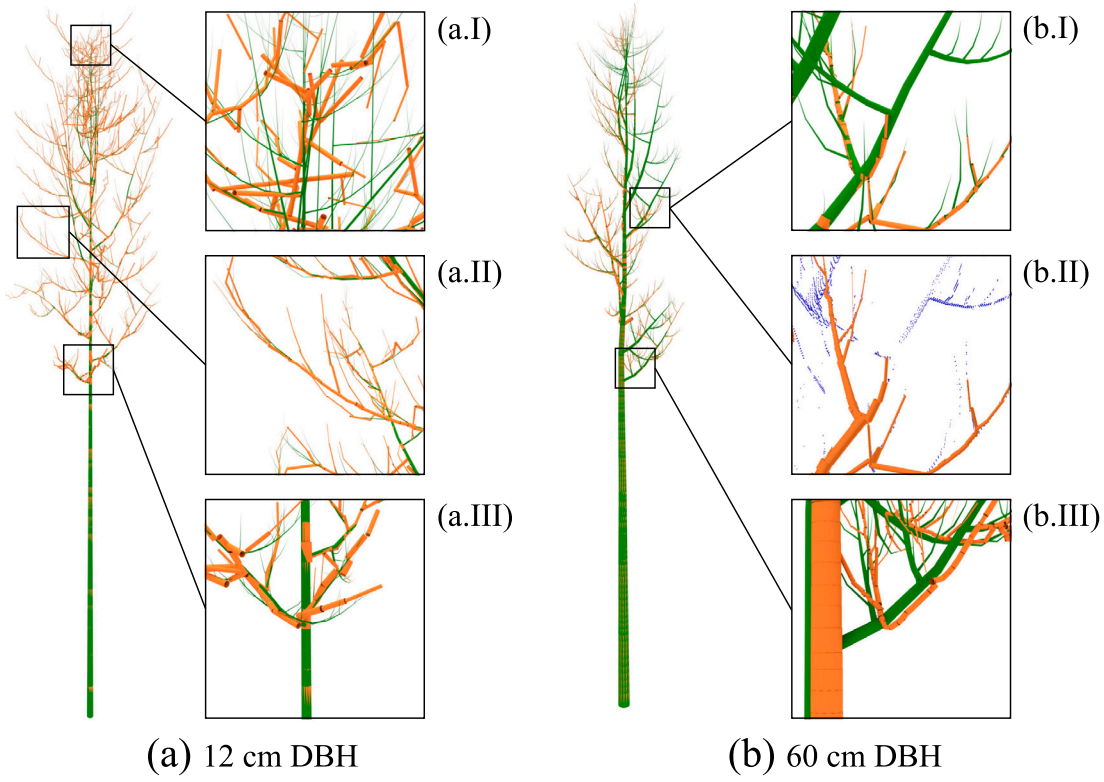

Fig. 8. Comparison of 3D tree model (green), QSM output (orange) and points (blue dots in panel b.II). (a) shows a tree with 12 cm DBH, a tree height of 14 m and a total tree volume of 0.07 m^3. The QSM estimation of small tree parts deviate by 65% from the (true) model volume and from the merchantable wood volume by 27%. Panel (a.I) show erroneous QSM cylinder fittings, (a.II) and (a.III) show that fitted cylinders are often slightly larger than the small branches, both due to a lack of sufficient points representing the branches. (b) shows a tree with 69 cm DBH, a tree height of 41 m and a total tree volume of 5.5 m^3. The QSM estimation of small tree parts deviate by −51% from the (true) model volume and by −3% from the merchantable wood volume. Panel (b.I) and (b.II) show the influence of occlusion, which leads to difficulties in consecutive cylinder fitting. In panel (b.III) the tree model and the QSM cylinders are slightly shifted for a better comparison between the tree model and the QSM output.

treeQSM is designed to estimate the volume (and other parameters) of any kind of tree-like structure, without constraints on a specific tree architecture. Hence, we are confident that the findings concerning limitations of volume estimation with TLS are realistic within our study constraints (e.g., tree model, stand structure and scanning system).

Computing resources for these TLS simulations were considerably high, in a way that access to a high-performance computer with several hundred CPUs is a requirement when calculation time should not exceed months.

The simulations show, that overall, the scanning system perform similar in volume estimation of the 3D tree models, with a bias in all volume estimates, however related to tree size or tree part size (see Fig. 5). This is especially the case when laser beam diameters are in a similar range for the different devices, as it is the case with most commonly used TLS devices in forest research (see Table 1). Most notably, the estimate of merchantable wood (diameter ≥ 7 cm) is considerably more precise (less variation) and accurate (less bias) than the volume estimates of small tree parts (small branches and tree top). According to Disney et al. (2012) and Calders et al. (2015) the tree volume estimates are dependent on the starting parameters of the treeQSM approach. Hence, as Fig. 5 implies, starting parameters as well as the volume estimation are much more sensitive to variation for small tree parts. In the case of accuracy, Raumonen et al. (2013) described an overestimation resulting from the treeQSM approach, whereas Calders et al. (2015) or Demol et al. (2022) observed this effect when comparing volume estimates with measurements of destructively sampled trees. The overestimation seems to originate from an overestimation of small tree parts. The reason for this effect becomes evident, when comparing the geometric scanning with the L-system in Fig. 3. The only TLS characteristics implemented in the L-system are prefiltering and distance noise. It seems, the distance noise leads to a severe overestimation of small tree parts, this is especially visible for the small branches and tree top (< 7 cm) but also in the merchantable wood estimates of smaller trees, up to about 25 cm DBH. Smaller trees are composed of small tree compartments, where a distance noise of 4 mm (as with the L-system, see Table 1) apparently has a considerable influence. The overestimation becomes even stronger, when there is additional mixed pixel noise, as implemented in the F-system (see Fig. 3). This noise effect increases when scanning small objects, owing to the increased common occurrence of edge (or mixed pixel) effects, i.e. a laser pulse intersecting with multiple objects and therefore possibly producing points away from an object's surface. Comparing the geometric system with the realistic ones, Fig. 4 shows the additional points due to the simulation of laser pulses with a certain diameter. These additional points originate from laser pulses, that did not hit the branches with their laser beam centre. As stated above, these additional points arise in a higher density on small branches. These noise effects, distance noise and mixed pixel noise, could lead to volume overestimation, because the branch diameter appears to be larger with noise. A visual analysis of the overlay of the 3D tree model with QSM cylinders, as displayed in the panels (a.I) to (a.III) in Fig. 8 reveal the overestimation of small tree parts. Often cylinders are relatively large compared to the branches they represent. In case of the R-system, which has mixed pixel and distance noise as well, multiple echo triggering and intensity filtering seem to alleviate the overestimation. Hence sophisticated ways of filtering point clouds, e.g. as demonstrated by Wilkes et al. (2021), could have a favourable effect on the volume estimation.

Another effect, counteracting to the overestimation due to noise, is missing information in point clouds, mostly due to occlusion but also due to angular resolution of the scanner and the distance of the object

to the scanner. This is clearly visible in Fig. 3 of the geometric scanning of small branches and tree top. This effect seems to be connected with tree size, where the tree crown becomes more complex and occlusion effects increase, i.e. Fig. 5 displays negative bias for large trees. The hypothesis for underestimation due to missing information in the point cloud is further supported by the analysis of Abegg et al. (2021), exploring the interaction of laser beam diameter and object size in TLS applications. The study demonstrated that small objects often lack a sufficient representation in the point cloud or are even completely invisible (occluded or not hit by a laser pulse due to scanner resolution), especially when situated at a large distance to the scanner and in a high density (e.g. in the tree crown). Fig. 8 with panels (b.I) and (b.II) shows an example where the gap in a point cloud leads to a stop in cylinder fitting, leaving a whole branch not considered by the QSM. The distance to "jump" over such gaps are part of the QSM parametrization.

Direct estimation of small tree parts from TLS point clouds, e.g. by the application of QSM, seems to be at its limit, due to either missing information in the point cloud or due to various noise effects. Nevertheless, small tree parts contribute far less to the total tree volume, reducing their biasing influence on the total tree volume (see Fig. 5 on the right hand side).

We were not able to see an effect of understorey density on the quality of the volume estimates from TLS point clouds, even with high densities of 32 000 understorey trees per hectare. The possible influence of understorey on the applied TLS systems is either occlusion, prefiltering, small distance deviation (some centimetres) on objects edges, or large distance deviation of the triggered laser echoes. The last of these effects arises when laser beams intersect with multiple objects with nearly the same amount of energy (only in F-system, as phase shift LiDAR). However, the setup of the forest scenes in this study was designed to allow an automatic clipping of the tree point clouds from the rest of the scene (i.e. clear separation of understorey layer from tree crowns and stem in the 3D models). That way, noise points, far from the tree crown or even close to the stem, were mostly clipped automatically from the tree point cloud. Therefore, a fraction of the distance noise did not interfere with the treeQSM for the volume estimation. Furthermore, the effect of occlusion and prefiltering (removing points based on ambiguous distance measurements), was not strong enough to reduce the quality of volume estimation systematically. A comparison of the point density on the tree surface as displayed in Fig. A.5 shows no visible difference between different understorey densities. 32 000 understorey trees per hectare result in even less than 4 pieces per m^2, which is not the highest density encountered in forests. Additionally, these virtual saplings did not carry leaves and were of a clear shape with small diameters leading to a rather low occlusion effect (see Fig. 1). Finally, real forest environments may also consist of coniferous understorey and scanning is sometimes performed during the leaf-on period; one would expect considerably stronger occlusion effects in such cases.

The combination of multiple scans from different locations is usually applied to mitigate the influence of occlusion (e.g. Watt and Donoghue, 2005; Hilker et al., 2012). In this study, the combination of point clouds from multiple scanning locations does not show a clear favourable effect on the bias of the volume estimates of large tree parts, as one would expect. This might be due to relatively low occlusion levels, without leaves or coniferous trees and other additional occluding factors occurring in real life scanning situations. However, a slight reduction in variability of the QSM estimates can be seen. On the other hand, there is a clear influence on the bias in the estimation of small tree parts, shifting the bias towards an overestimation with additional scan positions. Additionally, the variability in the volume estimates increases as the number of combined scanning locations increases. As Figs. A.1, A.2, A.3 and A.4 in the Appendix show, the increasing variability is due to the simulated realistic laser echo triggering system. As the realistic systems are subject to certain degree of uncertainty in distance measurement or introduce slight distance deviations at objects' edges, every additional scanning perspective adds noise according to the respective scanning direction to the object. The latter was described by Binney and Sukhatme (2009), whereas both noise effects are observed by many TLS practitioners. This additional noise in interaction with the treeQSM influences the outcome of the volume estimation, i.e., by connecting point cloud patches over "false" gaps (see Fig. 8). Furthermore, additional points from different scanner locations increase the density of noise, which could be interpreted as proper points from objects instead of being filtered out by the treeQSM algorithm.

The implemented realistic systems are based on laboratory experiments investigating the behaviour of TLS scanners when scanning edges of objects (Abegg et al., 2021). However, under real conditions there are many more factors influencing laser scanning, such as reflectance properties of the scanned objects, movement of the scanned trees and more complex "mixed pixel" situations than tested in the laboratory, some of them leading to further noise effects in the point cloud. We assume that in comparison with point clouds from real forest scenes retrieved with a real scanner of the same type as simulated, that the simulated point cloud is relatively clean. Hence, noise effects on volume estimation in real forests might be even higher than in this study.

The tree models used here do not represent the variety of existing trees, but rather a deciduous-tree-like structure without leaves. An application of TLS in forest inventories has to additionally handle coniferous trees and different branching structures. Furthermore, the stand structure in Switzerland, and elsewhere, can be far more complex than the single or double layered structure considered in this study, with an upper layer of adult trees and an understorey layer. The negative effects of TLS applications observed here are possibly even stronger when TLS is applied in a forest inventory. Nevertheless, we assume that noise effects and partly occlusion effects, however on a 'low' level, influencing the performance of treeQSM in volume estimation, as tested for stand and TLS specifications within this study, are similar to those observed in reality.

5. Conclusion

This simulation study strongly supports the findings of various authors that small branches are difficult to estimate with QSMs applied to TLS point clouds. The combination of multiple TLS scans even seem to exacerbate this effect in estimating volumes of small tree parts. On the other hand, volume estimates for merchantable wood of larger trees might be estimated with a small bias of a few percent of the total tree volume. Large trees (and large tree parts) contribute most to wood volume and biomass of forests, e.g. in Switzerland 79% of the stem volume of living trees is accounted for trees with DBH > 30 cm (Abegg et al., 2014). If future TLS research is able to find ways of estimating (merchantable) tree volume with an acceptable level of accuracy (and precision), TLS has the potential to become integrated in future NFI field campaigns. The way to go could be, understand the most important effects leading to bias (e.g. by simulation and comparison to real trees), finding ways to reduce the bias (e.g. by filtering, improved QSMs) or use TLS in enhanced allometric models.

Declaration of competing interest

The authors declare that they have no known competing financial interests or personal relationships that could have appeared to influence the work reported in this paper.

Data availability

Data will be made available on request.

Appendix

See Figs. A.1–A.5 and Tables A.1 and A.2.

Table A.1
Parameters used to define the tree model (description according to Weber and Penn (1995) and the add-on documentation) used for the main sample trees with volume estimation.

Parameter	Value	Parameter description
prune	True	boolean parameter indicating whether the tree should be pruned at a defined envelope
levels	4	number of branching levels
length	1, 0.3, 0.6, 0.45	relative length of child branch
lengthV	0, 0.05, 0.1, 0.02	variation in the relative length
branches	0, 30, 10, 10	number of branches per parent element on each level
curveRes	10, 7, 7, 3	curvature resolution of a tree element
curve	0, −50, 0, 0	angle of the end of the branch
curveV	10, 50, −30, 0	variation of curve
curveBack	0	curvature parameter to produce s-shaped branches
baseSplits	0	number of splits of the stem
segSplits	0	number of splits per branch
splitAngle	10, 10, 10, 0	angle of the branch splitting
splitAngleV	0	variation in the branch splitting
scale	from NFI data	tree height
scaleV	0	variation in the tree height
attractUp	−2	upward growth tendency
shape	8	general tree shape id
baseSize	from NFI data	fractional branchless area at tree base
ratio	from NFI data	ratio of the radius of the stem base to the tree height
taper	1	tapering of the stem and branches
ratioPower	1.2	reduction of the child branch diameter compared to parent branch/stem
downAngle	45, 45, 90, 45	angle between the child branch and the parent branch/stem
downAngleV	0, −50, 10, 10	variation in downAngle
rotate	140, 140, 140, 77	the angle of the child branch around the axis of the parent branch/stem
rotateV	20, 20, 20, 20	variation in rotate
scale0	1	trunk scaling
scaleV0	0.2	variation in scale0
pruneWidth	from NFI data	ratio of crown diameter to the tree height
pruneWidthPeak	0.2	location of the largest crown diameter
prunePowerHigh	0.05	shape of the upper part of the tree crown
prunePowerLow	1	shape of the lower part of the tree crown
pruneRatio	1	strength of pruning
bevelRes	4	the bevel resolution of the curves
resU	4	the resolution along the curves
startCurv	0	the angle between vertical and the starting direction

Table A.2
Parameters used to define the tree model (description according to Weber and Penn (1995) and the add-on documentation) for the trees composing the understorey layer.

Parameter	Value	Parameter description
prune	True	boolean whether the tree should be pruned at a defined envelope
levels	1, 2, 3	number of branching levels
length	1, 0.3, 0.6, 0.45	relative length of child branch
lengthV	0, 0, 0, 0	variation in the relative length
branches	0, 30, 10, 10	number of branches per parent element on each level
curveRes	10, 7, 7, 3	curvature resolution of a tree element
curve	0, −50, 0, 0	angle of the end of the branch
curveV	90, 90, −30, 0	variation in curve
curveBack	0	curvature parameter to produce s-shaped branches
baseSplits	0	number of splits of the stem
segSplits	0, 0, 0, 2	number of splits per branch
splitAngle	10, 10, 10, 10	angle of the branch splitting
splitAngleV	0	variation in the branch splitting
scale	defined as parameter	tree height
scaleV	0	variation in the tree height
attractUp	0.8	upward growth tendency
shape	7	general tree shape id
baseSize	0.5	fractional branchless area at tree base
ratio	0.03/10	ratio of the radius of the stem base to the tree height
taper	1	tapering of the stem and branches
ratioPower	1.2	reduction of the child branch diameter compared to parent branch/stem
downAngle	45, 45, 90, 45	angle between the child branch and the parent branch/stem
downAngleV	0, −50, 10, 10	variation in downAngle
rotate	140, 140, 140, 77	the angle of the child branch around the axis of the parent branch/stem
rotateV	0, 0, 10, 0	variation in rotate

(*continued on next page*)

Table A.2 (*continued*).

Parameter	Value	Parameter description
scale0	1	trunk scaling
scaleV0	0.2	variation in scale0
pruneWidth	0.2	ratio of crown diameter to the tree height
pruneWidthPeak	0.2	location of the largest crown diameter
prunePowerHigh	0.05	shape of the upper part of the tree crown
prunePowerLow	1	shape of the lower part of the tree crown
pruneRatio	1	strength of pruning
bevelRes	5	the bevel resolution of the curves
resU	4	the resolution along the curves
startCurv	0	the angle between vertical and the starting direction

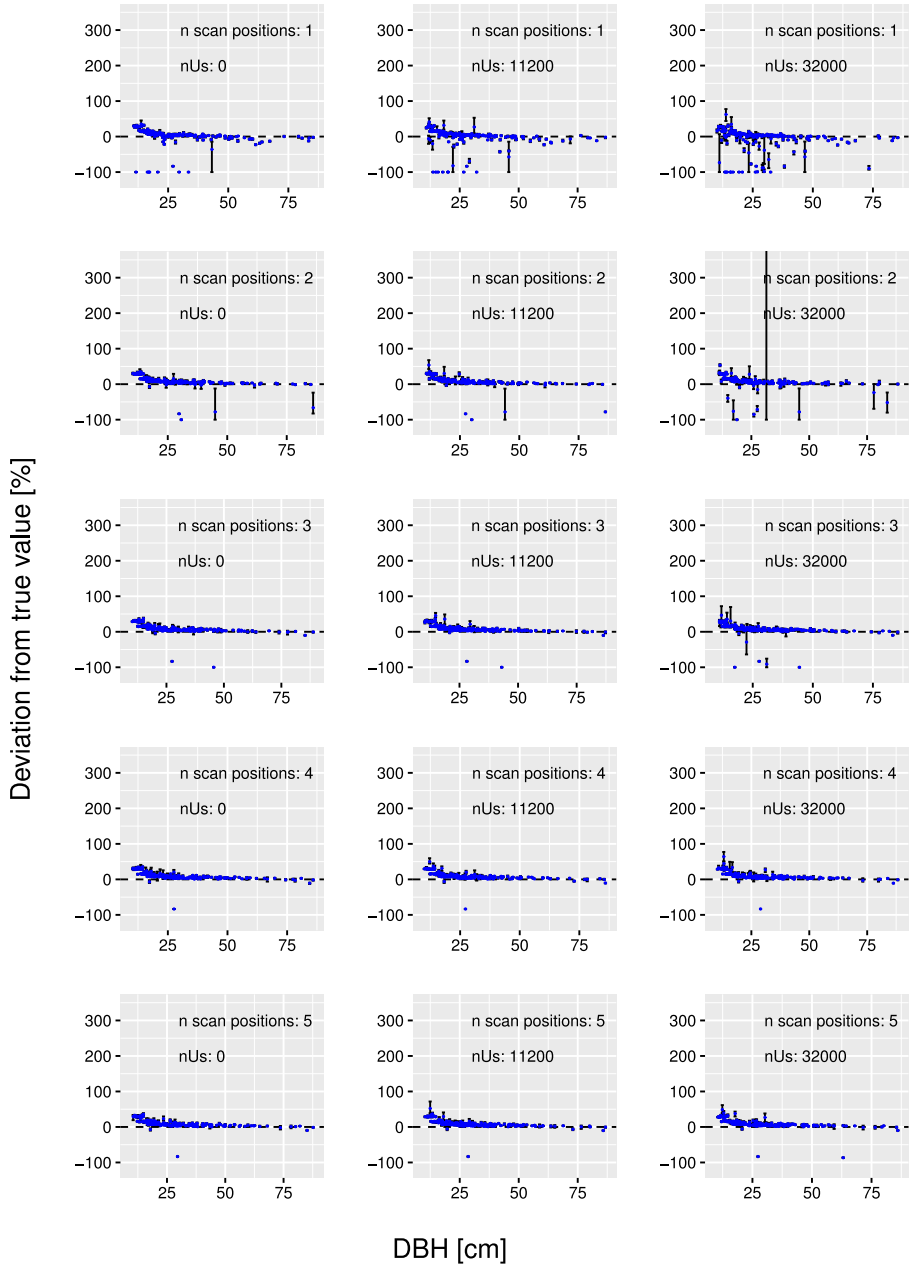

Fig. A.1. Bias of QSM volume estimates in simulated forest environments with geometric scanning for merchantable wood for different stem numbers of understorey trees per Hectare (nUs) and combined scanner locations (n scan positions). The blue dots represent the mean deviations of QSM volume estimates based on tree point clouds and the whiskers represent the range of volume estimates resulting from the use of different QSM starting parameters.

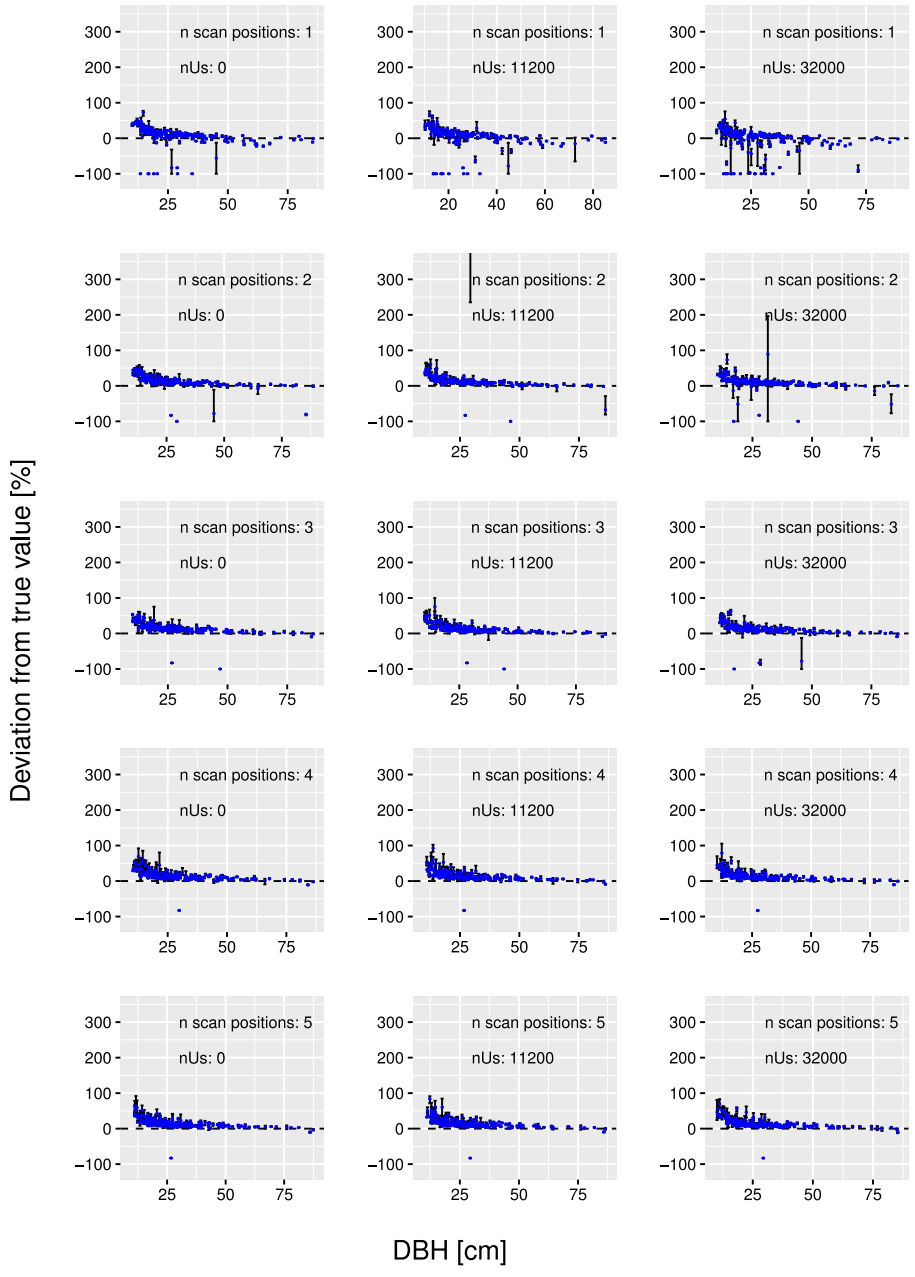

Fig. A.2. Bias of QSM volume estimates in simulated forest environments with L-system scanning for merchantable wood for different stem numbers of understorey trees per Hectare (nUs) and combined scanner locations (n scan positions). The blue dots represent the mean deviations of QSM volume estimates based on tree point clouds and the whiskers represent the range of volume estimates resulting from the use of different QSM starting parameters.

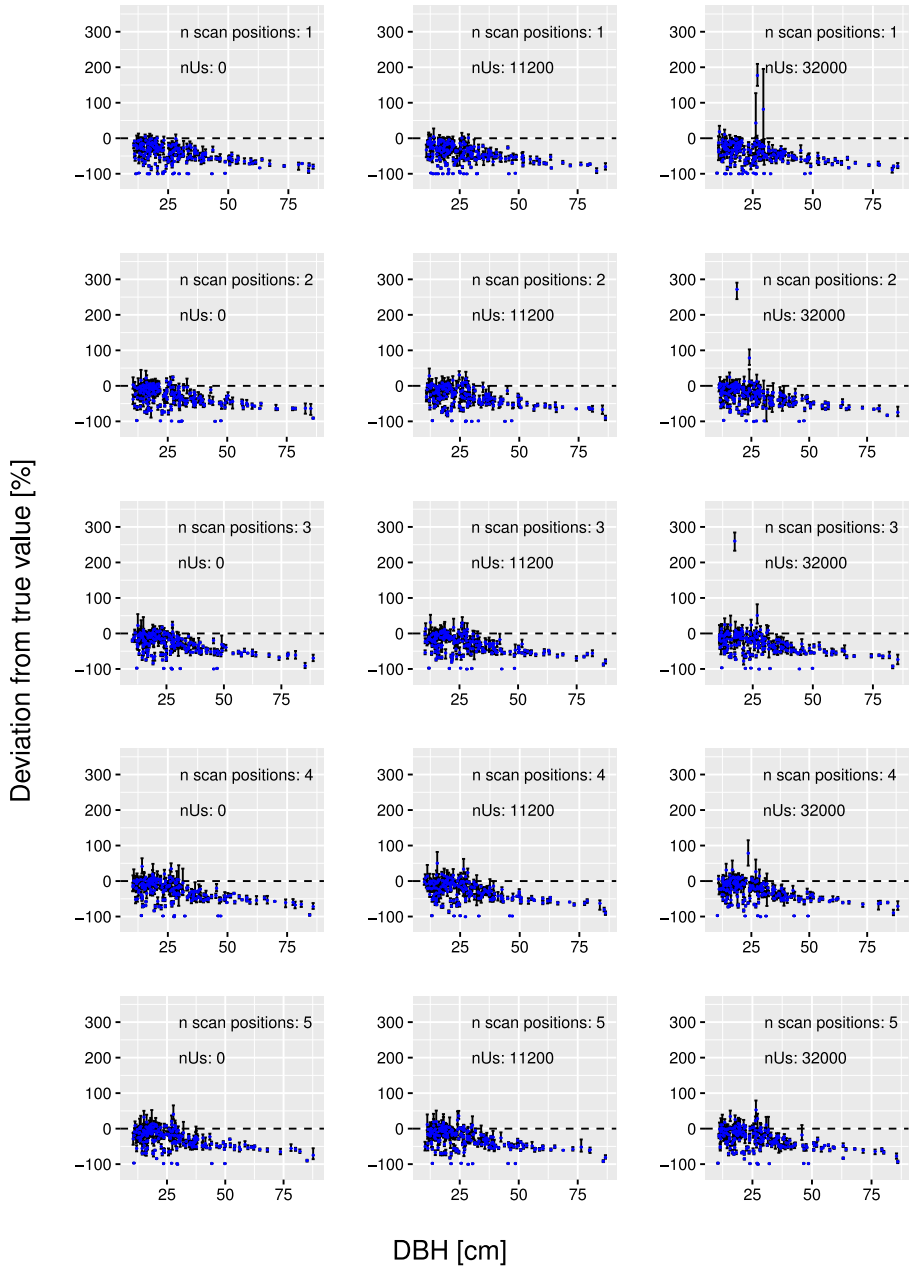

Fig. A.3. Bias of QSM volume estimates in simulated forest environments with geometric scanning for small tree parts (< 7 cm diameter) for different stem numbers of understorey trees per Hectare (nUs) and combined scanner locations (n scan positions). The blue dots represent the mean deviations of QSM volume estimates based on tree point clouds and the whiskers represent the range of volume estimates resulting from the use of different QSM starting parameters.

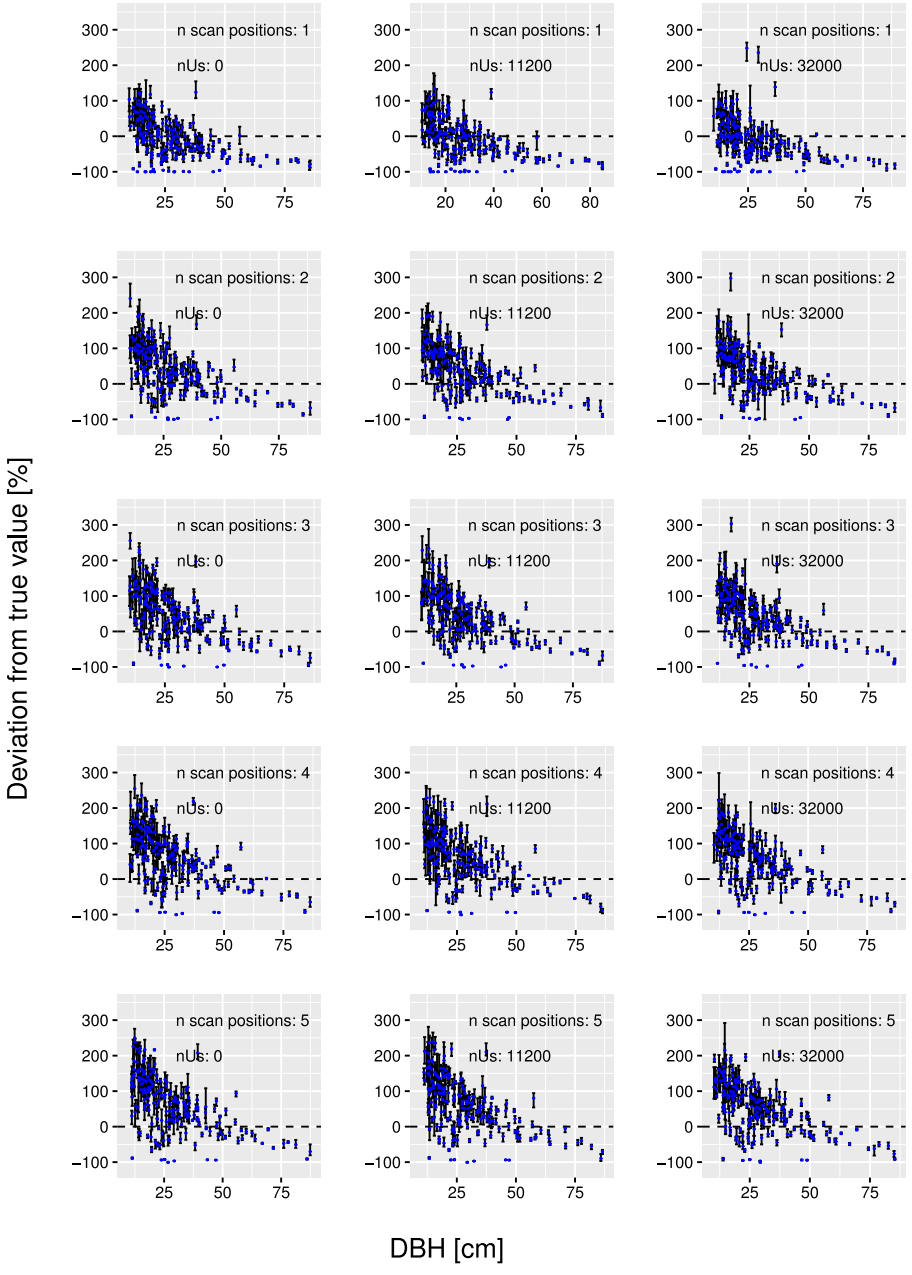

Fig. A.4. Bias of QSM volume estimates in simulated forest environments with L-system scanning for small tree parts (< 7 cm diameter) for different stem numbers of understorey trees per Hectare (nUs) and combined scanner locations (n scan positions). The blue dots represent the mean deviations of QSM volume estimates based on tree point clouds and the whiskers represent the range of volume estimates resulting from the use of different QSM starting parameters.

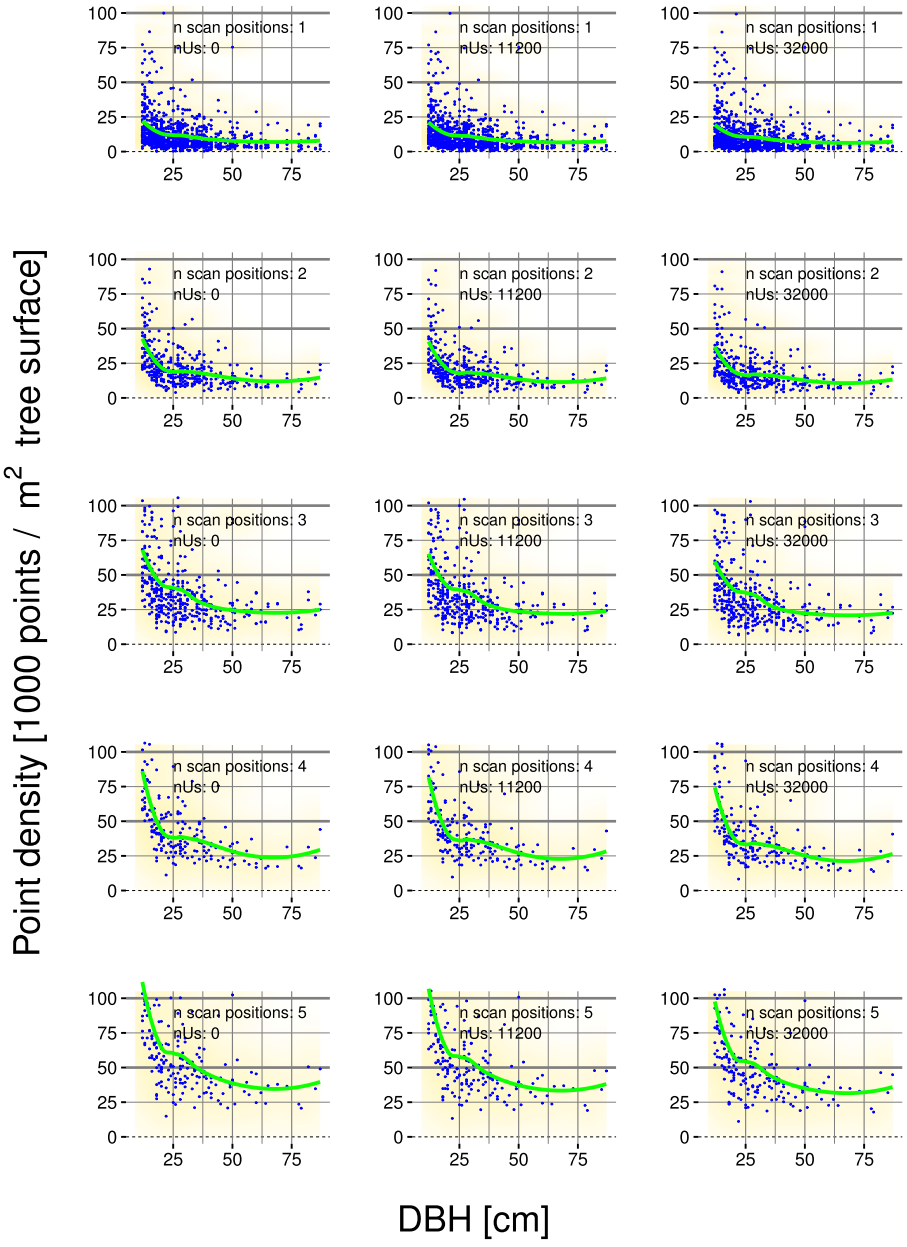

Fig. A.5. Point density on tree surface in simulated forest environments scanned with L-system for different stem number of understorey trees per Hectare (nUs) and combined scanner locations (n scan positions). The blue dots indicate the number of points on the tree surface (point density). The green line is a "loess" smoothing line on the data (R Core Team, 2017).

References

Abegg, M., Boesch, R., Schaepman, M.E., Morsdorf, F., 2021. Impact of beam diameter and scanning approach on point cloud quality of terrestrial laser scanning in forests. IEEE Trans. Geosci. Remote Sens. 59 (10), 8153–8167.

Abegg, M., Brändli, U.-B., Cioldi, F., Fischer, C., Herold-Bonardi, A., Huber, M., Keller, M., Meile, R., Rösler, E., Speich, S., Traub, B., Vidondo, B., 2014. Viertes schweizerisches landesforstinventar - ergebnistabellen und karten im internet zum lfi 2009–2013 (lfi4b). URL http://www.lfi.ch/resultate/anleitung.php.

Abegg, M., Kükenbrink, D., Zell, J., Schaepman, M.E., Morsdorf, F., 2017. Terrestrial laser scanning for forest inventories - tree diameter distribution and scanner location impact on occlusion. Forests 8 (184), 1–29.

Binney, J., Sukhatme, G.S., 2009. 3D tree reconstruction from laser range data. In: Robotics and Automation, ICRA'09 IEEE International Conference. Kobe, Japan.

Blender Online Community, 2015. Blender - A 3D Modelling and Rendering Package. Blender Foundation, Blender Institute, Amsterdam, URL http://www.blender.org.

Brassel, P., Lischke, H., 2001. Swiss National Forest Inventory: Methods and Models of the Second Assessment. WSL Swiss Federal Research Institute, Birmensdorf, Switzerland.

Brede, B., Calders, K., Lau, A., Raumonen, P., Bartholomeus, H., Herold, M., Kooistra, L., 2019. Non-destructive tree volume estimation through quantitative structure modelling: Comparing UAV laser scanning with terrestrial LiDAR. Remote Sens. Environ. 233.

Bremer, M., Rutzinger, M., Wichmann, V., 2013. Derivation of tree skeleton and error assessment using LiDAR point cloud data of varying quality. ISPRS J. Photogramm. Remote Sens. 80, 39–50.

Calders, K., Adams, J., Armston, J., Bartholomeus, H., Bauwens, S., Patrick Bentley, L., Chave, J., Danson, F.M., Demol, M., Disney, M., Gaulton, R., Moorthy, S.M.K., Levick, S.R., Saarinen, N., Schaaf, C., Stovall, A., Terryn, L., Wilkes, P., Verbeeck, H., 2020. Terrestrial laser scanning in forest ecology: Expanding the horizon. Remote Sens. Environ. 251. http://dx.doi.org/10.1016/j.rse.2020.112102.

Calders, K., Newnham, G., Burt, A., Murphy, S., Raumonen, P., Herold, M., Culvenor, D., Avitabile, V., Disney, M., Armston, J., Kaasalainen, M., 2015. Nondestructive estimates of above-ground biomass using terrestrial laser scanning. Methods Ecol. Evol. 6, 198–208.

Chave, J., Réjou-Méchain, M., Búrquez, A., Chidumayo, E., Colgan, M.S., Delitti, W.B., Duque, A., Eid, T., Fearnside, P.M., Goodman, R.C., Henry, M., Martínez-Yrízar, A., Mugasha, W.A., Muller-Landau, H.C., Mencuccini, M., Nelson, B.W., Ngomanda, A.,

Nogueira, E.M., Ortiz-Malavassi, E., Pélissier, R., Ploton, P., Ryan, C.M., Saldarriaga, J.G., Vieilledent, G., 2014. Improved allometric models to estimate the aboveground biomass of tropical trees. Global Change Biol. 20, 10.

Demol, M., Calders, K., Verbeeck, H., Gielen, B., 2021. Forest above-ground volume assessments with terrestrial laser scanning : A ground-truth validation experiment in temperate, managed forests. Ann. Bot. 128 (6), 805–819. http://dx.doi.org/10.1093/aob/mcab110.

Demol, M., Wilkes, P., Raumonen, P., Krishna Moorthy, S.M., Calders, K., Gielen, B., Verbeeck, H., 2022. Volumetric overestimation of small branches in 3D reconstructions of fraxinus excelsior. Silva Fennica 56, 1.

Disney, M., Kalogirou, V., Lewis, P., Prieto-Blanco, A., Hancock, S., Pfeifer, M., 2010. Simulating the impact of discrete-return LiDAR system and survey characteristics over young conifer and broadleaf forests. Remote Sens. Environ. 114, 1546–1560.

Disney, M., Lewis, P., Raumonen, P., 2012. Testing a new vegetation structure retrieval algorithm from terrestrial LiDAR scanner data using 3D models. In: Silvilaser 2012. No. SL2012-049. Vancouver, Canada. pp. 1–9.

FOREST EUROPE, 2015. State of Europe's forests 2015. FOREST Europe. URL http://www.foresteurope.org/docs/fullsoef2015.pdf.

Gastellu-Etchegorry, J.-P., Yin, T., Lauret, N., Cajgfinger, T., Gregoire, T., Grau, E., Feret, J.-B., Lopes, M., Guilleux, J., Dedieu, G., Malenovsky, Z., Cook, B.D., Morton, D., Rubio, J., Durrieu, S., Cazanave, G., Martin, E., Ristorcelli, T., 2015. Discrete anisotropic radiative transfer (dart 5) for modeling airborne and satellite spectroradiometer and LiDAR acquisitions of natural and urban landscapes. Remote Sens. 7 (2), 1667–1701.

Gschwandtner, M., Kwitt, R., Uhl, A., Pre, W., 2011. Blensor: Blender sensor simulation toolbox. In: Bebis, R., Boyle, B., Parvin, D., Koracin, R., Chung, Hammoud R. (Eds.), Advances in Visual Computing: 7th International Symposium, Vol. 6939/2011. ISVC 2011, Springer Verlag, Las Vegas, USA, pp. 199–208.

Hilker, T., Coops, N.C., Culvenor, D.S., Newham, G., Wulder, M.A., Bater, C.W., Siggins, A., 2012. A simple technique for co-registration of terrestrial LiDAR observations for forestry applications. Remote Sens. Lett. 3 (3), 239–247.

Keller, M., 2011. Swiss National Forest Inventory. Manual of the Field Survey 2004-2007. Swiss Federal Research Institute WSL, Birmensdorf, Switzerland, URL http://www.lfi.ch/publikationen/publ/anleitung3-en.php.

Kükenbrink, D., Gardi, O., Morsdorf, F., Thürig, E., Schellenberger, A., Mathys, L., 2021. Above-ground biomass references for urban trees from terrestrial laser scanning data. Ann. Botany 128 (6), 709–724. http://dx.doi.org/10.1093/aob/mcab002.

Kukko, A., Hyyppä, J., 2007. Laser scanner simulator for system analysis and algorithm development: A case with forest measurements. In: Laser Scanning 2007 and SilviLaser 2007.

Lau, A., Christopher, M., Batholomeus, H., Shenkin, A., Jackson, T., Malhi, Y., Herold, M., Bentley, L.P., 2019. Estimating architecture-based metabolic scaling exponents of tropical trees using terrestrial LiDAR and 3D modelling. Forest Ecol. Manag. 439, 132–145.

Lewis, P., 1999. Three-dimensional plant modelling for remote sensing simulation studies using the botanical plant modelling system. Agronomie 19 (3–4), 185–210.

Liang, X., Kankare, V., Hyyppä, J., Wang, Y., Kukko, A., Haggrén, H., Yu, X., Kaartinen, H., Jaakkola, A., Guan, F., Holopainen, M., Vastaranta, M., 2016. Terrestrial laser scanning in forest inventories. ISPRS J. Photogramm. Remote Sens. 115, 63–77.

Liu, C., Calders, K., Meunier, F., Gastellu-Etchegorry, J.-P., Nightingale, J., Disney, M., Origo, N., Woodgate, W., Verbeeck, H., 2022. Implications of 3D forest stand reconstruction methods for radiative transfer modeling: A case study in the temperate deciduous forest. J. Geophys. Res.: Atmos. 127.

Lovell, J., Jupp, D., Newnham, G., Coops, N., Culvenor, D., 2005. Simulation study for finding optimal LiDAR acquisition parameters for forest height retrieval. Forest Ecol. Manag. 214, 398–412.

MacDicken, K., Jonsson, O., Piña, L., Marklund, L., Maulo, S., Contessa, V., Adikari, Y., Garzuglia, M., Lindquist, E., Reams, G., D'Annunzio, R., 2016. Global Forest Resources Assessment 2015: How are the World's Forests Changing? Food and Agriculture Organistation of the United Nations (FAO), Roma, Italy.

Morsdorf, F., Nichol, C., Malthus, T., Woodhouse, I.H., 2009. Assessing forest structural and physiological information contentof multi-spectral LiDAR waveforms by radiative transfermodelling. Remote Sens. Environ. 113 (10), 2152–2163.

Pan, Y., Birdsey, R.A., Fang, J., Houghton, R., Kauppi, P.E., Kurz, W.A., Phillips, O.L., Shvidenko, A., Lewis, S.L., Canadell, J.G., Ciais, P., Jackson, R.B., Pacala, S.W., McGuire, A.D., Piao, S., Rautiainen, A., Sitch, S., Hayes, D., 2011. A large and persistent carbon sink in the world's forests. Science 333, 988–993.

Pitkänen, T.P., Raumonen, P., Kangas, A., 2019. Measuring stem diameter with TLS in boreal forests by complementary fitting procedure. ISPRS J. Photogramm. Remote Sens. 147, 294–306.

R Core Team, 2017. R: A Language and Environment for Statistical Computing. R Foundation for Statistical Computing, Vienna, Austria, URL https://www.R-project.org/.

Raumonen, P., Kaasalainen, M., Akerblom, M., Kaasalainen, S., Kaartinen, H., Vastaranta, M., Holopainen, M., Disney, M., Lewis, P., 2013. Fast automatic precision tree models from terrestrial laser scanner data. Remote Sens. 5, 491–520.

Raumonen, P., Kaasalainen, S., Kaasalainen, M., Kaartinen, H., 2011. Approximation of volume and branch size distribution of trees from laser scanner data. In: ISPRS Workshop Laser Scanning 2011. In: Vol. XXXVIII-5/W12 of International Archives of the Photogrammetry, Remote Sensing and Spatial Information Sciences, Calgary, Canada, pp. 79–84.

Saarinen, N., Kankare, V., Vastaranta, M., Luoma, V., Pyörälä, J., Tanhuanpää, T., Liang, X., Kaartinen, H., Kukko, A., Jaakkola, A., Yu, X., Holopainen, M., Hyyppä, J., 2017. Feasibility of terrestrial laser scanning for collecting stem volume information from single trees. ISPRS J. Photogramm. Remote Sens. 123, 140–158.

Trochta, J., Kral, K., Janik, D., Adam, D., 2013. Arrangement of terrestrial laser scanner positions for area-wide stem mapping of natural forests. Can. J. Forest Res. 43, 355–363.

Van der Zande, D., Hoet, W., Jonckheere, I., van Aardt, J., Coppin, P., 2006. Influence of measurement set-up of ground-based LiDAR for derivation of tree structure. Agricult. Forest Meteorol. 141, 147–160.

Van der Zande, D., Jonckheere, I., Stuckens, J., Verstraeten, W.W., Coppin, P., 2008. Sampling design of ground-based LiDAR measurements of forest canopy structure and its effect on shadowing. Can. J. Remote Sens. 34 (6), 526–538.

Wang, D., Puttonen, E., Casella, E., 2022. Plantmove: A tool for quantifying motion fields of plant movements from point cloud time series. Int. J. Appl. Earth Observ. Geoinformation 110 (102781), http://dx.doi.org/10.1016/j.jag.2022.102781.

Watt, P.J., Donoghue, D.N.M., 2005. Measuring forest structure with terrestrial laser scanning. Int. J. Remote Sens. 26, 1437–1446.

Weber, J., Penn, J., 1995. Creation and rendering of realistic trees. In: SIGGRAPH '95 Proceedings of the 22nd Annual Conference on Computer Graphics and Interactive Techniques. pp. 119–128.

Wezyk, P., Koziol, K., Glista, M., Pierzchalski, M., 2007. Terrestrial laser scanning versus traditional forest inventory, first result from the polish forests. In: ISPRS Workshop on Laser Scanning 2007 and SilviLaser, Vol. 2007. pp. 424–429.

Wilkes, P., Shenkin, A., Disney, M., Malhi, Y., Patrick Bentley, L., Boni Vicari, M., 2021. Terrestrial laser scanning to reconstruct branch architecture from harvested branches. Methods Ecol. Evol. 1–14.

Yang, X., Strahler, A.H., Schaaf, C.B., Jupp, T., Zhao, F., Wang, Z., Culvenor, D.S., Newnham, G.J., Lovell, J., Dubayah, R.O., Woodcock, C.E., Ni-Meister, W., 2013. Three-dimensional forest reconstruction and structural parameter retrievals using a terrestrial full-waveform LiDAR instrument (echidna). Remote Sens. Environ. 135, 36–51.

Zhang, C., Chen, T., 2001. Efficient feature extraction for 2D/3D objects in mesh representation. In: Proceedings 2001 International Conference on Image Processing.